Numerical simulations of pulsatile blood flow using a new constitutive model.

Jiannong Fang
GEOLEP-ICARE-ENAC,
Ecole Polytechnique Fédérale de Lausanne,
1015 Lausanne, Switzerland

and

Robert G. Owens*
Département de mathématiques et de statistique,
Université de Montréal,
CP 6128 succ. Centre-Ville,
Montréal QC H3C 3J7, Canada

February 22, 2006

Abstract

In the present paper we use a new constitutive equation for whole human blood [21] to investigate the steady, oscillatory and pulsatile flow of blood in a straight, rigid walled tube at modest Womersley numbers. Comparisons are made with the experimental results of Thurston [38] for the pressure drop per unit length against volume flow rate and oscillatory flow rate amplitude. Agreement in all cases is very good. In the presentation of the numerical and experimental results we discuss the microstructural changes in the blood that account for its rheological behaviour in this simple class of flows. In this context, the concept of an apparent complex viscosity proves to be useful.

Keywords: aggregation, viscoelastic, thixotropic, pulsatile flow, Womersley, complex viscosity.

1. Introduction

The principal explanation for the non-Newtonian character of human blood is to be found in the aggregration, disaggregation, deformation, orientation and mi-

*Corresponding author. Address: Département de mathématiques et de statistique, Université de Montréal, CP 6128 succ. Centre-Ville, Montréal QC H3C 3J7, Canada. Tel: + 1 (514) 343 2315. Fax: +1 (514) 343 5700. Email: owens@dms.umontreal.ca

gration of the erythrocytes. Although flow conditions in the heart and healthy arterial system are such as to justify describing the equations of motion using the Navier-Stokes equations (see, for example, [16]), the unwelcome presence of a stenosis or an aneurysm, for example, might be expected to lead to recirculatory regions being established in the cardiovascular system where red cell aggregration and thus, non-uniform viscosity, are possible. The blunting along the vessel axis of symmetry of the usual (steady) Hagen-Poiseuille or (unsteady) Womersley velocity profiles in narrow glass tubes is a manifestation of shear-thinning and is due to wall-induced migration and cell aggregation (see, for example, the discussion on pages 391-394 of [6]). This might be expected to be reproduced in the smaller vessels of the human blood vessel network, although (to the authors' knowledge) this has not yet been measured with any success *in vivo*. For useful recent reviews on state of the art experimental methods for measuring velocity profiles and calculating wall shear stresses in human aortic and cardiac flows *in vivo*, papers by Taylor and Draney [36] and Steinman and Taylor [34] are to be recommended.

The variations in local viscosity seen in flowing blood may be accounted for in steady shear flows using generalized Newtonian or Casson-type models [7], where in both constitutive descriptions the fluid is inelastic and the extra-stress tensor in some non-linear relationship with the rate of strain tensor. An empirical constitutive model that has enjoyed some popularity over the past three decades is that of Walburn and Schneck [40]. This is a power-law type model relating the elastic stress to the shear rate, hematocrit and total protein minus albumin content. The predictions of the model were compared with those of a Newtonian fluid, Casson model and Bingham model for both steady and pulsatile laminar flow through a straight tube by Rodkiewicz et al. [31] in 1990. The Walburn and Schneck model was seen to give markedly different results from the other models in pulsatile flow and these were stated as being in conformity with some experimental results [17]. The authors noted that the constitutive model of Walburn and Schneck was developed for low shear rates, however, and was not valid for certain shear rate regimes seen in their pulsatile flow simulations. We further note that no yield stress, viscoelasticity or thixotropy is to be seen in the Walburn and Schneck model although the original authors raised doubts about the existence of a yield stress in blood in dynamic situations [40]. Details of a recent comparison between a Newtonian, Casson, power-law and Quemada [25] model are to be found in the paper of Neofytou [20]. The author considered the case of channel flow where part of one of the channel walls was forced to oscillate laterally, this being claimed to reproduce some flow phenomena seen under realistic arterial conditions. The Casson and Quemada models were seen to agree well in their predictions and were preferred over the power-law model which has an unbounded viscosity at zero shear-rate.

In 2000 Zhang and Kuang [45] surveyed and tested several inelastic constitutive models for blood. Parameters for each model were determined by using a weighted least-squares method to fit the steady experimental data consisting of the angular velocity of the outer cylinder and the shear stress on the inner cylinder of a coaxial cylinder rheometer. Both canine and human blood was

used in the experiments. The authors roughly divided up the models into those of Casson and power-law type. In the former category the K-L equation [18] and the Quemada equation [26] were found to give best agreement with the laboratory measurements. In the latter category (which included the Walburn and Schneck [40] model, discussed above) a bi-exponent viscosity model

$$\eta = \eta_e + \eta_D \exp\left(-\sqrt{t_D\dot{\gamma}}\right) + \eta_A \exp\left(-\sqrt{t_A\dot{\gamma}}\right),$$

(t_A, t_D being time scales and $\dot{\gamma}$ the shear rate) was claimed to give best results. It is apparent that none of the models tested is viscoelastic or thixotropic, although some of the models of Casson type feature a yield stress. Our expectations of such models, therefore, is that they would be limited, in general, to steady flows.

Recently, a generalized Newtonian model was used by El-Khatib and Damiano [14] for the simulation of pulsatile blood flow in cylindrical tubes of radii between 8×10^{-4}m and 9×10^{-3}m at a frequency of 1Hz and at hematocrits varying between 0.1 and 0.8. Differences could be seen in the non-Newtonian and Womersley velocity profiles, these becoming more obvious as the hematocrit was increased. Disparity in the amplitude and phase of the wall shear rates for the Newtonian and non-Newtonian models became progressively greater as the ratio of the steady and oscillatory pressure gradient amplitudes decreased to zero (purely oscillatory flow). Such scenarios were conjectured to be possible for blood flow in large vessels *in vivo*. Little time variation was seen in the viscosity across the tube diameter during the simulations, but the appearance of unphysical "spikes" in the viscosity profile at certain points in time when the shear rate was sufficiently low, revealed the weakness of using a viscosity law that was an instantaneous function of the shear rate and led the authors to proposed a viscosity function that depended on radial position alone.

None of the above models takes account of the viscoelasticity and thixotropy of blood. Viscoelastic constitutive models suitable for describing blood have been proposed recently by Yeleswarapu [43, 44] and by Anand and Rajagopal [1] (the latter being developed in the context of the general thermodynamic framework of Rajagopal and Srinivasa [30]). The model of Anand and Rajagopal [1] gave good agreement with the experimental data of Thurston [38] in steady Poiseuille flow and oscillatory tube flow and comparisons were made with the results from the Yeleswarapu model and both generalized Oldroyd-B and Maxwell models (also derived within the framework of [30]). Neither of the generalized models was found to give satisfactory results for oscillatory flows. The authors stated that the triangular shear rate experimental results of Bureau et al. [5] could be verified with their model but, unfortunately, this was not demonstrated in their paper. For a discussion of thixotropic effects in blood, see [15], for example. One consequence of the viscosity depending on time as well as the local shear rate is that the "spiking" referred to in the previous paragraph should not occur. See the results in Figs. 6 and 8 in the present paper in support for this contention.

The purpose of this paper is to gain some rheological insight into the observed macroscopic behaviour of blood in pulsatile flows. The model used in the present paper was presented in detail in [21] although, for completeness, we outline

some of the main steps in the derivation in Section 2.1.. The constitutive model is viscoelastic, shear-thinning and thixotropic. It bears some similarities to earlier work by authors such as Quemada [27, 28, 29], Williams et al. [41] and De Kee and co-workers [8, 35]. The common outcome of the modelling done by all these authors was a generalized Maxwell-type equation for the stress due to the rouleaux. Both viscosity and relaxation time are functions of a structure variable n (say) which, in the papers cited above, is either the number fraction of red blood cells in aggregates (more generally, aggregated particles) [8, 27, 28, 29, 35] or of aggregated cell faces [41]. In the model used in the present paper the structure variable upon which both a shear viscosity and a relaxation time depend is the average aggregate size. For simplicity the number density of the erythrocytes is assumed constant, although a Navier-type slip condition is introduced to account for cell migration and, indeed, shown to be essential to get quantitative agreement with experimental results.

In this paper the proposed model is used to numerically predict the components of the applied pressure gradient that are in phase and in quadrature with the volume flow rate amplitude in oscillatory and pulsatile flow in a straight tube. The flow geometry is admittedly simple, but the flow regimes studied give rise to some rich and fascinating rheological phenomena. In Section 3. we detail the governing equations and describe a simple finite difference scheme for their resolution. Numerical results for steady, oscillatory and pulsatile flow are presented in Section 4. and very good agreement with the experimental results of Thurston [38] is achieved. In 4.2. an interpretation of the pressure gradient results for small amplitude oscillatory flow is shown to be possible by calculating the complex viscosity components of an equivalent linear viscoelastic fluid. Results are also presented to show how the average aggregate size, polymeric viscosity and axial velocity profiles vary as functions of the radial position over an oscillatory cycle.

2. Governing equations

The macroscopic equations of motion for blood may be written

$$\rho \frac{D\boldsymbol{v}}{Dt} = -\nabla p + \eta_N \nabla^2 \boldsymbol{v} + \nabla \cdot \boldsymbol{\tau}, \tag{1}$$

$$\nabla \cdot \boldsymbol{v} = 0, \tag{2}$$

where, in the usual notation, ρ denotes the fluid density, $\boldsymbol{v}$ the fluid velocity, p is the pressure, η_N is the (Newtonian) plasma viscosity and $\boldsymbol{\tau}$ is an elastic stress tensor, this latter taking account of the contribution of the erythrocytes to the total Cauchy stress.

2.1. A new constitutive equation for blood

To close the system of equations (1)-(2) we require a constitutive equation for $\boldsymbol{\tau}$ and for this we will extend the use of the very recent model of Owens [21] to non-homogeneous flows (that is, for which $\nabla \boldsymbol{v} \neq \mathbf{0}$). A typical distribution of erythrocyte aggregates of various sizes at some instant in time is depicted in Fig.

1. We represent an erythrocyte by a dumbbell and say that the dumbbell is of *type* k if it belongs to an aggregate of k dumbbells (this latter being henceforth referred to as a $k-$mer). Let $\psi_k(\boldsymbol{x}, \boldsymbol{q}, t)d\boldsymbol{x}d\boldsymbol{q}$ be the number of dumbbells of type k having centre of mass with position vector between $\boldsymbol{x}$ and $\boldsymbol{x} + d\boldsymbol{x}$ and an end-to-end vector between $\boldsymbol{q}$ and $\boldsymbol{q} + d\boldsymbol{q}$ at time t. Integrating ψ_k over all configuration space we then get

$$\int_{\boldsymbol{q}} \psi_k(\boldsymbol{x}, \boldsymbol{q}, t)d\boldsymbol{q} = kN_k(\boldsymbol{x}, t), \tag{3}$$

where $N_k(\boldsymbol{x}, t)$ denotes the number density of $k-$mers.

To arrive at an evolution equation for ψ_k, Owens [21] followed ideas drawn from the classical theory of network models for viscoelastic fluids. In the model developed in [21] the erythrocytes were represented in their capacity to be transported, stretched and orientated in a flow by Hookean dumbbells. Denoting the diameter of an erythrocyte by d (approximately $8.5\mu m$) and a macroscopic length scale by L (a vessel diameter, say), it may be shown that the assumption (valid in the larger blood vessels) $d/L \ll 1$ leads to a continuity equation for ψ_k of the form

$$\frac{D\psi_k}{Dt} = -\frac{\partial}{\partial \boldsymbol{q}} \cdot \left(\nabla \boldsymbol{v} \cdot \boldsymbol{q}\psi_k - \frac{2k_BT}{\zeta_k}\frac{\partial \psi_k}{\partial \boldsymbol{q}} - \frac{2\boldsymbol{q}H}{\zeta_k}\psi_k \right) + C - D, \tag{4}$$

where C and D are creation and destruction functionals, respectively. The assumption $d/L \ll 1$ allows for the neglect in the bulk flow of the diffusion term in real space that would otherwise be present in (4) and justifies considering the velocity of the centre of mass of an erythrocyte to be that of the plasma at that point. From the terms in the parentheses on the right-hand side of (4) we identify k_B as Boltzmann's constant, T the absolute temperature, H the Hookean spring constant and ζ_k as the (k-dependent) drag coefficient. The three terms in parentheses arise from the velocity-space averaged rate of change of the conformation vector $\boldsymbol{q}$ when acceleration terms are neglected. The first of the three terms arises from a linear Taylor expansion of the difference in the bead velocities of a dumbbell. A truncated series of this type is justified under the assumption $d/L \ll 1$. The last two terms in the parentheses are, respectively, a smoothed Brownian force (accounting for the pressure difference between the haemoglobin solution inside the erythrocyte and the plasma outside) and a spring force (accounting for the tension in the bounding elastic membrane of the erythrocyte).

For the creation and destruction terms, Owens [21] assumed, as is usual in network theory, that formation/ aggregation is a Brownian process and that the rate is proportional to the equilibrium distribution, leading to an expression for C in (4) of the form $h_k(\dot{\gamma}, t)\psi_{k,0}$ for some rate coefficient h_k. He also assumed that the rate of breakdown of networks of a given number of cells is proportional to the number of those cells, leading to $D = g_k(\dot{\gamma}, t)\psi_k$ for some fragmentation rate coefficient g_k. Arguments were then put forward to establish the precise

form of g_k and h_k:

$$g_k(\dot{\gamma},t) = \frac{b(\dot{\gamma})(k-1)}{2} + a(\dot{\gamma})\sum_{j=1}^{\infty} N_j, \tag{5}$$

$$h_k(\dot{\gamma},t) = \frac{a(\dot{\gamma})}{2N_{k,0}}\sum_{i=1}^{k-1} N_i N_{k-i} + \frac{b(\dot{\gamma})}{N_{k,0}}\sum_{j=1}^{\infty} N_{k+j}, \tag{6}$$

and, as a consequence, the following continuity equation for ψ_k may be written down:

$$\begin{aligned}\frac{D\psi_k}{Dt} =& -\frac{\partial}{\partial \boldsymbol{q}}\cdot\left(\nabla \boldsymbol{v}\cdot\boldsymbol{q}\psi_k - \frac{2k_BT}{\zeta_k}\frac{\partial\psi_k}{\partial\boldsymbol{q}} - \frac{2\boldsymbol{q}H}{\zeta_k}\psi_k\right) + h_k\psi_{k0} - g_k\psi_k,\\ =& -\frac{\partial}{\partial \boldsymbol{q}}\cdot\left(\nabla \boldsymbol{v}\cdot\boldsymbol{q}\psi_k - \frac{2k_BT}{\zeta_k}\frac{\partial\psi_k}{\partial\boldsymbol{q}} - \frac{2\boldsymbol{q}H}{\zeta_k}\psi_k\right)\\ &+ \frac{a(\dot{\gamma})\psi_{k0}}{2N_{k0}}\sum_{i=1}^{k-1} N_i N_{k-i} + \frac{b(\dot{\gamma})\psi_{k0}}{N_{k0}}\sum_{j=1}^{\infty} N_{k+j}\\ &- \frac{b(\dot{\gamma})(k-1)}{2}\,\psi_k - a(\dot{\gamma})\psi_k\sum_{j=1}^{\infty} N_j.\end{aligned} \tag{7}$$

In (7), $a(\dot{\gamma})$ and $b(\dot{\gamma})$ are an aggregation rate and a degradation rate, respectively, and dependent on the local shear rate

$$\dot{\gamma} = \sqrt[+]{\frac{1}{2}\dot{\boldsymbol{\gamma}} : \dot{\boldsymbol{\gamma}}}, \tag{8}$$

where $\dot{\boldsymbol{\gamma}} = \nabla \boldsymbol{v} + \nabla \boldsymbol{v}^T$ is the rate-of-strain tensor.

2.1.2. Macroscopic rate equations

Using (3) it may be seen that dividing the continuity equation (7) throughout by k and integrating over configuration space leads to an evolution equation (a generalized Smoluchowski equation) for N_k, the number density of $k-$mers:

$$\begin{aligned}\frac{DN_k}{Dt} =& \frac{a(\dot{\gamma})}{2}\sum_{i=1}^{k-1} N_i N_{k-i} + b(\dot{\gamma})\sum_{j=1}^{\infty} N_{k+j}\\ &- \frac{b(\dot{\gamma})(k-1)}{2}N_k - a(\dot{\gamma})N_k\sum_{j=1}^{\infty} N_j.\end{aligned} \tag{9}$$

(In deriving (9) we have used the divergence theorem and the boundary conditions $\partial\psi_k/\partial n \longrightarrow 0$, and $\psi_k \longrightarrow 0$ as $|\boldsymbol{q}| \longrightarrow \infty$.)

To derive the macroscopic rate equation for the number density of aggregates $M = \sum_{k=1}^{\infty} N_k$ we sum (9) from $k = 1$ to ∞ and assume that all required sums

are convergent to get

$$\frac{DM}{Dt} = \frac{D}{Dt}\sum_{k=1}^{\infty} N_k = -\frac{a(\dot\gamma)}{2}\sum_{k=1}^{\infty}\sum_{j=1}^{\infty} N_k N_j + \frac{b(\dot\gamma)}{2}\sum_{k=1}^{\infty}(k-1)N_k,$$
$$= -\frac{a(\dot\gamma)}{2}M^2 + \frac{b(\dot\gamma)}{2}(N_0 - M), \tag{10}$$

where N_0 denotes the number density of all erythrocytes and is given by $N_0 = \sum_{k=1}^{\infty} kN_k$. To arrive at (10) we have used the case $a_{i,j} = 1$ of the following easily verifiable results, valid for all matrices $\boldsymbol{A}$ having (i,j)th component $a_{i,j}$:

$$\sum_{k=1}^{\infty}\sum_{i=1}^{k-1} a_{i,k-i}N_i N_{k-i} = \sum_{k=1}^{\infty}\sum_{j=1}^{\infty} a_{k,j}N_k N_j, \tag{11}$$

$$\sum_{k=1}^{\infty}\sum_{j=1}^{\infty} a_{k,j}N_{k+j} = \sum_{k=1}^{\infty}\sum_{i=1}^{k-1} a_{i,k-i}N_k. \tag{12}$$

We now multiply (9) throughout by k, sum from $k = 1$ to ∞ and use the formulae (11)-(12) in the case $a_{i,j} = (i + j)$ to get

$$\frac{DN_0}{Dt} = \frac{D}{Dt}\sum_{k=1}^{\infty} kN_k = -\frac{a(\dot\gamma)}{2}\sum_{k=1}^{\infty}\sum_{j=1}^{\infty}(k-j)N_k N_j + \frac{b(\dot\gamma)}{2}\sum_{k=1}^{\infty}\sum_{j=1}^{\infty}(k-j)N_{k+j} = 0. \tag{13}$$

This last result demonstrates that the number density of erythrocytes in the model is constant along fluid particle trajectories and that, therefore, in a material volume the total number of erythrocytes is constant.

Finally, using (10) and (13) we may easily write down a differential equation for the average size density $n = N_0/M$ of an aggregate:

$$\frac{Dn}{Dt} = -\frac{N_0}{M^2}\frac{DM}{Dt} = \frac{N_0}{M^2}\left(\frac{1}{2}a(\dot\gamma)M^2 - \frac{1}{2}b(\dot\gamma)(N_0 - M)\right)$$
$$= \frac{1}{2}a(\dot\gamma)N_0 - \frac{1}{2}b(\dot\gamma)n^2 + \frac{1}{2}b(\dot\gamma)n. \tag{14}$$

2.1.2. A single mode constitutive equation for $\boldsymbol{\tau}$.

A Kramers expression for the elastic extra-stress $\boldsymbol{\tau}_k$ due to the N_k $k-$mers is (see, for example, [4])

$$\boldsymbol{\tau}_k = H\int_{\mathbb{R}^3} \boldsymbol{qq}\psi_k(\boldsymbol{x},\boldsymbol{q},t)\, d\boldsymbol{q} - kN_k k_B T\boldsymbol{I}. \tag{15}$$

By multiplying the continuity equation (7) throughout by $\boldsymbol{qq}$ and integrating over configuration space, Owens [21] obtained a closed-form constitutive equation for $\boldsymbol{\tau}_k$ in the form

$$\boldsymbol{\tau}_k + \left(\frac{4H}{\zeta_k} + g_k\right)^{-1}\overset{\triangledown}{\boldsymbol{\tau}}_k = kN_k k_B T\left(\frac{4H}{\zeta_k} + g_k\right)^{-1}\dot{\boldsymbol{\gamma}}, \quad k = 1,2,3,\ldots, \tag{16}$$

where ∇ denotes the upper convected derivative

$$\overset{\nabla}{\boldsymbol{B}} := \frac{\partial \boldsymbol{B}}{\partial t} - \nabla \boldsymbol{v} \boldsymbol{B} - \boldsymbol{B} \nabla \boldsymbol{v}^T. \tag{17}$$

The coefficient of the upper convected derivative of $\boldsymbol{\tau}_k$ in (16) is a relaxation time and is seen to be smaller than the usual Maxwell time $\zeta_k/4H$ due to the supplementary relaxation mechanism involved in the fragmentation process of cell aggregates. Rather than using a multi-mode model (which would necessitate a spectrum of relaxation times), Owens [21] summed up all equations (16) from $k = 1$ to ∞ and justified the use of a single, representative relaxation time

$$\mu = \frac{n\lambda_H}{1 + g_n n \lambda_H}, \tag{18}$$

to get

$$\boldsymbol{\tau} + \mu \overset{\nabla}{\boldsymbol{\tau}} = N_0 k_B T \mu \dot{\boldsymbol{\gamma}}, \tag{19}$$

where $\boldsymbol{\tau} = \sum_{k=1}^{\infty} \boldsymbol{\tau}_k$.

2.1.2. Rate functions $a(\dot{\gamma})N_0$ and $b(\dot{\gamma})$.

From (14) we see that

$$a(\dot{\gamma})N_0 = 2 \left. \frac{Dn}{Dt} \right|_{n=1}.$$

Since we expect that all aggregates break up as the shear rate is increased sufficiently, it is anticipated that $n \longrightarrow 1$ and $Dn/Dt \longrightarrow 0$ as $\dot{\gamma} \longrightarrow \infty$, and that therefore $a(\dot{\gamma})N_0 \longrightarrow 0$ as $\dot{\gamma} \longrightarrow \infty$. At shear rates up to some critical value (where fragmentation effects start to counterbalance coagulation) we further expect that the rate of rouleau formation will be an increasing function of shear rate (strictly positive at equilibrium) due to the increased rate of collisions between aggregates that is implied in this case. Although, seemingly, the exact form of the $a(\dot{\gamma})N_0$ curve is not known (either experimentally or theoretically) we may deduce, therefore, that if $a(\dot{\gamma})N_0$ is a continuous function, a maximum is attained at some critical value $\dot{\gamma}_c$ of shear rate (estimated by Murata and Secomb [19] to be $\dot{\gamma}_c \approx 5.78 s^{-1}$ for human blood at an hematocrit of 0.45) before the function decays monotonically to zero with further increases in shear rate. Further discussion may be found in the paper of Chen and Huang [9] and experimental evidence for our contentions is furnished by Shiga et al. [33] who measured aggregation rates for human erythrocytes at low hematocrits over a range of shear rates using a cone and plate viscometer.

Motivated by the work of Murata and Secomb [19], we choose a simple form for $a(\dot{\gamma})N_0$:

$$a(\dot{\gamma})N_0 = \begin{cases} c_1 + c_2\dot{\gamma}, & \dot{\gamma} \leq \dot{\gamma}_c \\ (c_1 + c_2\dot{\gamma}_c)\frac{\dot{\gamma}_c}{\dot{\gamma}}, & \dot{\gamma} \geq \dot{\gamma}_c, \end{cases} \tag{20}$$

where c_1 and c_2 are positive parameters, to be determined.

3. Pulsatile flow in a tube

We assume that a solution $(\boldsymbol{v}, p, \boldsymbol{\tau})$ to pulsatile blood flow in a rigid and uniform pipe of radius R (say) exists in the form

$$\boldsymbol{v} = (0, 0, v_z(r,t)),\ \boldsymbol{\tau} = \boldsymbol{\tau}(r,t),\ \frac{\partial p}{\partial z} = \frac{\partial p}{\partial z}(t). \tag{21}$$

The assumed form of the velocity leads to the convective part of the material derivative $\boldsymbol{v} \cdot \nabla \equiv 0$. The $z-$ component of the equation of linear momentum (1) and the (r,z) component of the constitutive equation (19) then simplify to

$$\rho \frac{\partial v_z}{\partial t} = \frac{1}{r}\frac{\partial}{\partial r}\left(r T_{rz}\right) - \frac{\partial p}{\partial z}, \tag{22}$$

and

$$\tau_{rz} + \mu \frac{\partial \tau_{rz}}{\partial t} = N_0 k_B T \mu \frac{\partial v_z}{\partial r}, \tag{23}$$

respectively, where, in (22) T_{rz} is the (r,z) component of the extra-stress tensor $\boldsymbol{T}$ and related to τ_{rz} by

$$T_{rz} = \eta_N \frac{\partial v_z}{\partial r} + \tau_{rz}. \tag{24}$$

We follow Thurston [38] in integrating (22) over a disk of radius R, to get

$$\rho \frac{\partial}{\partial t} \int_{\theta=0}^{2\pi} \int_{r=0}^{R} v_z r dr d\theta = \int_{\theta=0}^{2\pi} \int_{r=0}^{R} \frac{1}{r}\frac{\partial}{\partial r}\left(r T_{rz}\right) r dr d\theta - \int_{\theta=0}^{2\pi} \int_{r=0}^{R} \frac{\partial p}{\partial z} r dr d\theta. \tag{25}$$

This leads to

$$\rho \frac{\partial U_T}{\partial t} = 2\pi R T_{rz}(R,t) + \pi R^2 P, \tag{26}$$

where U_T denotes the volume flow rate and $P = -\partial p/\partial z$. We decompose the solution to (26) into a steady and oscillatory part thus:

$$U_T = U_s + \widetilde{U},\ P = P_s + \widetilde{P},\ T_{rz}(R,t) = T_s(R) + \widetilde{T}_{rz}(R,t),$$

where $(U_s, T_s(R), P_s)$ denotes the steady solution to (26) and the terms with a tilde denote the time-dependent part of the solution.

Suppose that the complex form of the oscillatory part of the imposed pressure gradient is

$$\widetilde{P} = P_M \exp(i\omega t), \tag{27}$$

for some (real) amplitude P_M. Then, seeking oscillatory solutions for the wall shear stress and the volume flow rate of the form

$$\widetilde{T}_{rz}(R,t) = T^*_{rz} \exp(i\omega t), \tag{28}$$

$$\widetilde{U} = U^* \exp(i\omega t), \tag{29}$$

where T^*_{rz} and U^* are complex amplitudes, we may integrate (26) over one period $2\pi/\omega$ to get

$$P_s = -\frac{2}{R} T_s(R), \tag{30}$$

and, subtracting this from (26) leads to

$$\rho\frac{\partial\widetilde{U}}{\partial t} = 2\pi R\widetilde{T}_{rz}(R,t) + \pi R^2\widetilde{P}. \tag{31}$$

Let us write the complex amplitudes T^*_{rz} and U^* in (28)-(29) in terms of their real and imaginary parts as $T^*_{rz} = T'_{rz} + iT''_{rz}$ and $U^* = U' + iU''$. Then, from (28)-(29) and (31) we see that these satisfy

$$-\omega\rho U'' = 2\pi RT'_{rz} + \pi R^2 P_M, \tag{32}$$

$$\omega\rho U' = 2\pi RT''_{rz}. \tag{33}$$

(Note that in the paper of Thurston [38] it is the volume flow rate that is prescribed. However, Anand and Rajagopal [1] prescribe the pressure gradient, as we do in the present paper, which seems to us to be more natural). Taking real parts of (29) we get

$$\begin{aligned}\widetilde{U} &= (U'\cos\omega t - U''\sin\omega t),\\ &= \sqrt{U'^2+U''^2}\left(\frac{U'}{\sqrt{U'^2+U''^2}}\cos\omega t - \frac{U''}{\sqrt{U'^2+U''^2}}\sin\omega t\right),\\ &= U_M\cos(\omega t + A),\end{aligned} \tag{34}$$

where U_M denotes the amplitude of the volume flow rate oscillations and A is the phase difference with the oscillatory part of the imposed pressure gradient, satisfying

$$\tan A = \frac{U''}{U'}.$$

Using the same notation as Anand and Rajagopal [1] and Thurston [38], we may write the oscillatory part of the pressure gradient $\widetilde{P}$ in the complex form

$$\widetilde{P} = P^*_M\exp(i(\omega t + A)), \tag{35}$$

with a complex amplitude P^*_M written in terms of its real and imaginary parts as

$$P^*_M = P'_M + iP''_M.$$

Equating the real parts of (27) and (35) then yields

$$\widetilde{P} = P_M\cos\omega t = P'_M\cos(\omega t + A) - P''_M\sin(\omega t + A), \tag{36}$$

where P'_M and $-P''_M$ may be understood to be, respectively, the amplitudes of the oscillatory pressure gradient components in phase and in quadrature with the volume flow rate, and given by

$$P'_M = P_M\cos A,\ -P''_M = P_M\sin A. \tag{37}$$

To calculate P_M' and P_M'' we first prescribe P_s and P_M and then solve (23) for the stress, coupled with

$$\begin{aligned}\rho\frac{\partial v_z}{\partial t} &= \frac{1}{r}\frac{\partial}{\partial r}(rT_{rz}) + P_s + P_M\cos\omega t,\\ &= \eta_N\frac{1}{r}\frac{\partial}{\partial r}\left(r\frac{\partial v_z}{\partial r}\right) + \frac{1}{r}\frac{\partial}{\partial r}(r\tau_{rz}) + P_s + P_M\cos\omega t,\end{aligned} \tag{38}$$

in $r \in (0, R)$, over some time interval taken to be sufficiently long that the oscillatory parts of the wall shear stress and volume flow rate become periodic in time and may be expressed in the form (28)-(29), respectively. For the problem to be well-posed, suitable initial and inflow conditions must be prescribed for the solution of the elastic stress τ_{rz} and (38) is solved subject to the boundary and initial conditions

$$\frac{\partial v_z}{\partial r}(0,t) = 0, \tag{39}$$

$$v_z(r,0) = V_z(r), \tag{40}$$

$$v_z(R,t) = -\beta\tau_{rz}, \tag{41}$$

where $V_z(r)$ is, (for example) the velocity for the steady problem and β is a non-negative slip coefficient. The reason for allowing slip on the boundary is now explained below.

With the convective part of the material derivative in unsteady Poiseuille flow (21) identically zero we see that the evolution equation (13) for the number density of erythrocytes collapses to

$$\frac{\partial N_0}{\partial t} = 0,$$

so that if N_0 is initially chosen to be a constant (dependent on the hematocrit) it remains so at all subsequent times. In the remainder of this paper, therefore, and with a view to simplicity, we set N_0 equal to a constant everywhere in the flow. In reality, there would be wall-induced migration of the red blood cells, leading to a non-uniform distribution of these cells across a vessel diameter and, in particular, to a cell-depleted region near the vessel walls. To properly model this migration effect we would have had to have included a diffusion term in physical space in the continuity equation (4) for ψ_k and made the configuration space of a dumbbell dependent on the distance of its centre of mass from the walls: a formidable undertaking! The Navier slip condition (41) has been introduced to mimic the lubrication effect of the cell-depleted region.

3.1. Steady shear viscosity and parameter determination

From (18) and (19) we may write down the steady-state viscosity in the form

$$\eta(\dot\gamma) = \frac{N_0 k_B T\lambda_H n_{st}}{1 + g_{n_{st}} n_{st}\lambda_H}, \tag{42}$$

where n_{st} denotes the steady-state value of the average aggregate size density n. We simplify (42) by first observing that in any steady flow where the convective derivative is identically zero, such as steady Poiseuille or Couette flow, (14) becomes

$$0 = \frac{1}{2}a(\dot{\gamma})N_0 - \frac{1}{2}b(\dot{\gamma})n_{st}^2 + \frac{1}{2}b(\dot{\gamma})n_{st}, \tag{43}$$

so that, from (5) we may deduce that $g_{n_{st}}n_{st} = \frac{1}{2}n_{st}(n_{st}-1) + aMn_{st} = \frac{3}{2}a(\dot{\gamma})N_0$.

The observations above allow us to write

$$\eta(\dot{\gamma}) = \frac{\eta_\infty n_{st}}{1 + \frac{3}{2}a(\dot{\gamma})N_0\lambda_H}, \tag{44}$$

where we have used the behaviour of n and $a(\dot{\gamma})N_0$ as $\dot{\gamma} \longrightarrow \infty$ (see the discussion in Section 2.1.2.) to identify $N_0 k_B T \lambda_H$ with the infinite shear-rate viscosity η_∞. Rearranging (42), we may express the steady-state value of n as a function of shear-rate:

$$n_{st} = \frac{\eta(\dot{\gamma})}{\eta_\infty}\left(1 + \frac{3}{2}a(\dot{\gamma})N_0\lambda_H\right), \tag{45}$$

and then find $b(\dot{\gamma})$ from (43)

$$b(\dot{\gamma}) = \frac{a(\dot{\gamma})N_0}{n_{st}(n_{st}-1)}. \tag{46}$$

There are numerous studies in the experimental literature on the steady-state viscosity for blood (see, for example, the Couette data of Chien et al. [10, 11]) and to the available steady shear data we may fit a Cross model [12]

$$\eta(\dot{\gamma}) = \eta_0\left(\frac{1 + \theta\dot{\gamma}^m}{1 + \xi\dot{\gamma}^m}\right), \tag{47}$$

where η_0 is the zero-shear rate viscosity, m is a power law and θ and ξ are parameters related by $\theta/\xi = \eta_\infty/\eta_0$. Fig. 2 shows the fit with the Couette data of Chien [10] using the steady viscosity model (47) and parameter values as supplied in Appendix A. Combining (45) and (47) leads to

$$n_{st} = \frac{\eta_0}{\eta_\infty}\left(\frac{1 + \theta\dot{\gamma}^m}{1 + \xi\dot{\gamma}^m}\right)\left(1 + \frac{3}{2}a(\dot{\gamma})N_0\lambda_H\right). \tag{48}$$

If we subtract (43) from (14) we get

$$\frac{\partial n}{\partial t} = -\frac{1}{2}b(\dot{\gamma})(n - n_{st})(n + n_{st} - 1). \tag{49}$$

Since $b(\dot{\gamma})$ is chosen as a positive function of $\dot{\gamma}$ we may deduce from (49) that

1. $\partial n/\partial t < 0$ if $n > n_{st}$ and, conversely, $\partial n/\partial t > 0$ if $n < n_{st}$, so that at shear rate $\dot{\gamma}$, $n \longrightarrow n_{st}(\dot{\gamma})$ as $t \longrightarrow \infty$,

2. the greater the absolute difference in value between n and n_{st} the more rapid the rate of change of n,

3. breakup of aggregates ($\partial n/\partial t < 0$) occurs over shorter time scales than coagulation ($\partial n/\partial t > 0$).

We note that although only a partial time derivative appears on the left-hand side of (49), n is a function both of radial position and time.

The choice of parameter values for m, η_0, η_∞ and ξ used in the present paper are reported in Appendix A.

3.2. Numerical scheme

We solve (23), (38) and (49) numerically for τ_{rz}, v_z and n using a simple staggered finite difference scheme in space ($0 < r < R$) and a Runge-Kutta method in time. Let r_i ($i = 0, \ldots, N$) denote the ith finite difference node in the radial direction, where $r_i = i\Delta r$ and Δr is the finite difference step R/N, as shown in Figure 3. Then, denoting a finite difference approximation to a variable at the ith node with the superscript i, our discretization of (38) is

$$\frac{dv_z^i}{dt} = \frac{1}{\rho}\left[\frac{T_{rz}^{i+\frac{1}{2}} - T_{rz}^{i-\frac{1}{2}}}{\Delta r} + \frac{T_{rz}^{i+\frac{1}{2}} + T_{rz}^{i-\frac{1}{2}}}{2r_i} + P\right], \qquad i = 1, \ldots, N-1, \quad (50)$$

where $T_{rz}^{i+\frac{1}{2}} = \tau_{rz}^{i+\frac{1}{2}} + \eta_N \frac{v_z^{i+1} - v_z^i}{\Delta r}$. v_z^0 is obtained by discretizing the symmetry boundary condition (39) using a second-order finite difference approximation and the Navier slip condition (41) is imposed by first extrapolating τ_{rz} to the wall of the tube. $\tau_{rz}^{i+\frac{1}{2}}$ (evaluated at the midpoint between node i and $i+1$) is given by

$$\frac{d\tau_{rz}^{i+\frac{1}{2}}}{dt} = \frac{1}{\mu^{i+\frac{1}{2}}}\left[N_0 k_B T \mu^{i+\frac{1}{2}}\left(\frac{v_z^{i+1} - v_z^i}{\Delta r}\right) - \tau_{rz}^{i+\frac{1}{2}}\right], \qquad i = 0, \ldots, N-1, \quad (51)$$

where $n^{i+\frac{1}{2}}$ is obtained from

$$\frac{dn^{i+\frac{1}{2}}}{dt} = -\frac{1}{2} b(\dot{\gamma}^i)(n^{i+\frac{1}{2}} - n_{st}^{i+\frac{1}{2}})(n^{i+\frac{1}{2}} + n_{st}^{i+\frac{1}{2}} - 1), \qquad i = 0, \ldots, N-1, \quad (52)$$

and where the shear rate at the ith node is defined by $\dot{\gamma}^i = \left|\frac{v_z^{i+1} - v_z^i}{\Delta r}\right|$. The coupled ordinary differential equations (50)-(52) are then solved, subject to suitable initial conditions for v_z^i, $\tau_{rz}^{i+\frac{1}{2}}$ and $n^{i+\frac{1}{2}}$, using a fifth-order Runge-Kutta method with adaptive time step.

4. Numerical results

For all computed results presented in this Section, there was a common set of parameter values, some physically motivated (fluid density, zero- and high shear-rate elastic viscosities, plasma viscosity) and others, such as the parameters m

and ξ in (47) and c_1, c_2 in (20), were selected to best fit the experimental data. The values given to these parameters are supplied in Appendix A. The tube radius R was set equal to 0.43×10^{-3}m in keeping with the choice of Thurston [38]. In his paper, Thurston worked with the root mean square (rms) value U instead of U_M (see equation (34)). Suppose that the rms value is calculated over one period, T (say). Then we have the relation

$$U = \sqrt{\frac{1}{T}\int_0^T U_M^2 \cos^2\left(\frac{2\pi t}{T}\right) dt} = \frac{\sqrt{2}}{2} U_M \approx 0.707 U_M. \tag{53}$$

Similarly, rather than working with the in phase and in quadrature components P'_M and $-P''_M$ of $\widetilde{P}$ (see (36)) Thurston presented results for their rms values, denoted hereafter by P' and $-P''$.

4.1. Steady flow

The results presented in Fig. 4 show the numerically and experimentally [38] determined pressure drop per unit length P_s against the volume flow rate for steady flow. Both the no-slip ($\beta = 0$) and slip condition ($\beta = 0.002$) cases are plotted and provide convincing evidence of the need in the present model of introducing slip on the vessel boundary to get quantitative agreement with the experimental data. See the end of Section 3. for a discussion. The slip condition, not surprisingly, reduces the pressure drop per unit length required to maintain a given flow rate when compared to the no-slip case. Poiseuille's law for a Newtonian fluid would predict a straight line graph and although the relationship between P_s and U_s is seen to be linear for the lowest values of U_s, a transition to a non-linear regime, marking the start of shear-thinning behaviour, may be seen at $U_s \approx 2 \times 10^{-5}\text{cm}^3\text{s}^{-1}$.

4.2. Oscillatory flow

In Figs. 5(a)-(c) we present the computed and experimental [38] rms values of the real and imaginary parts of the complex negative pressure gradient amplitude P^*_M against the rms amplitude of the volume flow rate oscillations, in the case that U_s, T_s and P_s are all zero. The upper sets of curves in all three figures show the variation of P' with U and the lower set, in keeping with the data presentation of Thurston [38], show $-P''$ to the left of the curve minimum (at $U \approx 2.5 \times 10^{-3}\text{cm}^3\text{s}^{-1}$) and P'' to the right. In reality, therefore, P'' passes from being negative to positive as U increases from $10^{-3}\text{cm}^3\text{s}^{-1}$ to $10^{-2}\text{cm}^3\text{s}^{-1}$. The experimental results of Figs. 5(a) and (c) are those presented in Fig. 5 of the paper of Thurston [38] and those in Fig. 5(b), those shown in Fig. 3 of the same paper. It may be conjectured that the differences in the experimental data between Figs. 5(a) or (c) and Fig. 5(b) are due to experimental error, memory effects and/or changes in the rheology of the blood samples between one experiment and another. In the numerical results, a no-slip condition ($\beta = 0$) has been imposed in Fig. 5(a), whereas slip in the axial velocity on the walls $r = R$ has been allowed in Figs. 5(b) and (c). In addition to reducing the computed

value of $-P''$ for the smallest values of U and bringing it into closer agreement with Thurston's results [38], the use of a non-zero slip parameter in (41) is seen to be necessary to accurately capture the cross-over point in P''.

Let us express the $z-$component of the velocity in complex form as $v_z = v_z^*(r)\exp(i\omega t)$ where v_z^* is a complex function of r and related to the complex volume flow rate amplitude U^* (see Eqn. (29)) by

$$U^* = 2\pi \int_{r=0}^{R} v_z^*(r)\, r\, dr. \tag{54}$$

Then the complex form of the shear stress (24) may be written in the form

$$T_{rz} = T_{rz}^* \exp(i\omega t) = \left(\eta_N + \frac{N_0 k_B T \mu}{1 + i\omega\mu}\right) \frac{\partial v_z}{\partial r} = \eta_v^* \frac{dv_z^*}{dr} \exp(i\omega t), \tag{55}$$

where the complex viscosity η_v^* is a function of shear-rate and time. In order to better understand Figs. 5(a)-(c) it is useful to consider the very small ($U \ll 1$) amplitude oscillatory solution of (38) for a linear viscoelastic fluid having the same rms volume flow rate amplitude U for the same values of P' and P'' as in our non-linear model. The complex extra-stress $\boldsymbol{T}_{lv}$ for the linear viscoelastic model, is then expressed in terms of the rate of strain tensor as

$$\boldsymbol{T}_{lv} = \eta^* \dot{\boldsymbol{\gamma}}, \tag{56}$$

where $\eta^* = \eta' - i\eta''$ is what we shall term the *apparent complex viscosity*. η' is the so-called apparent dynamic viscosity and relates to the part of the stress in phase with the rate of strain. η'' is related to the storage modulus and is the elastic component of the complex viscosity. In classical (Newtonian) fluid mechanics η' is just the (constant) coefficient of viscosity η_N and $\eta'' = 0$. If, in addition to assuming small amplitude oscillatory flow, we further assume that the Womersley number

$$\alpha = R\sqrt{\rho\omega/|\eta^*|}, \tag{57}$$

and non-dimensionalized slip parameter $\delta = \beta|\eta^* - \eta_N|/R$ are both small (< 1) we may then show (see Appendix B for details) that the rms in phase and in quadrature pressure gradient amplitudes for a linear viscoelastic fluid are related to U by

$$P'_M = \frac{8U_M}{\pi R^4}\left[\eta' - \frac{4\beta}{R}(\eta'^2 - \eta''^2 - \eta_N\eta') - \frac{\rho\omega\beta R}{3}\eta''\right], \tag{58}$$

$$P''_M = \frac{8U_M}{\pi R^4}\left[-\eta'' + \frac{\rho\omega R^2}{6} + \frac{4\beta}{R}(2\eta' - \eta_N)\eta'' - \frac{\rho\omega\beta R}{3}(\eta' - \eta_N)\right]. \tag{59}$$

The relations (58)-(59) generalise those obtained by Thurston [38] (Eqn. (10)) for a linear viscoelastic fluid with the no-slip condition ($\beta = 0$). The Womersley number α may be interpreted as a ratio of unsteady inertial forces to viscous forces.

From (58)-(59) we see that for a Newtonian fluid (η' a positive constant, $\eta'' = 0$), both P' and P'' would be positive and their graphs straight lines with positive slopes passing through the origin. That the graphs of P' and P'' are not straight lines therefore demonstrates clearly the non-Newtonian character of blood. In Fig. 5(b) P'' is negative for U smaller than about $2.5 \times 10^{-3}\text{cm}^3\text{s}^{-1}$ and the reason for this is the important viscoelastic character of blood for small U. Otherwise stated, the sum of the terms in parentheses which multiply U in (59) is negative for η'' sufficiently large. The balance of the terms changes with increasing U and the behaviour of the blood becomes less elastic. To quantify the relative importance of the viscous and elastic contributions to the apparent complex viscosity we use (58)-(59) and the data in Fig. 5(c) to calculate that $\eta' = 1.4244 \times 10^{-2}$Pa s and $\eta'' = 2.8671 \times 10^{-2}$ Pa s at an rms volume flow rate amplitude of $U = 1.2772 \times 10^{-5}\text{cm}^3\text{s}^{-1}$. The corresponding Womersley number is then $\alpha = 0.2765$ and the magnitude of the dimensionless slip coefficient is $|\delta| = 0.1469$. At an rms volume flow rate amplitude of $U = 9.63 \times 10^{-3}\text{cm}^3\text{s}^{-1}$ the components of the complex viscosity are determined from the data in Fig.5(c) to be $\eta' = 5.3140 \times 10^{-3}$Pa s and $\eta'' = 2.5779 \times 10^{-4}$ Pa s with corresponding Womersley number $\alpha = 0.6783$ and slip coefficient magnitude $|\delta| = 0.0201$. We note, therefore, that as U increases from $1.2772 \times 10^{-5}\text{cm}^3\text{s}^{-1}$ to $9.63 \times 10^{-3}\text{cm}^3\text{s}^{-1}$ the ratio between the apparent viscosities η' and η'' increases by a factor of approximately 41.5. This means that the loss angle (phase difference between stress and strain) is also increasing in the linear viscoelastic model, indicating less elastic behaviour. These observation are in agreement with those made by Thurston [38] and by Vlastos et al. [39] in their study of blood in small amplitude oscillatory shear flows.

In Fig. 6 (a)-(f) we plot snapshots of the average aggregate size n, the polymeric viscosity $N_0 k_B T \mu$ and the axial velocity v_z as functions of the tube radius at four equally spaced points in time during a complete oscillatory cycle. The figures in the left hand column correspond to an rms volume flow rate amplitude of $U = 1.2772 \times 10^{-5}\text{cm}^3\text{s}^{-1}$ and those on the right to an rms volume flow rate amplitude of $U = 9.63 \times 10^{-3}\text{cm}^3\text{s}^{-1}$. Although the local shear rate is changing with time everywhere except along the axis of symmetry, as evidenced in Figs. 6(e) and (f), very little change over a cycle is visible in either n or μ. This is because, although both are dependent on the local shear rate, the aggregates do not have time over the course of a cycle to break up and reform. This is therefore a thixotropic effect. The reader is referred at this point to the discussion in the Introduction on the problems of using a viscosity function that changes instantaneously with the shear rate. It may be seen that the effect of a higher volume flow rate amplitude is to reduce the average aggregate size and the polymeric viscosity at each radial position r. The distribution of n also becomes more skewed towards the centreline, with increasing U. A weakness of the present formulation is that the erythrocyte number density N_0 is a constant. Were particle migration to take place, it might be expected that the concentration of red blood cells near the centreline would be greater than in the present simulations and, assuming that packing attained some maximum value, that the viscosity function would have zero radial derivative at $r = 0$.

4.3. Pulsatile flow

The effect of adding a steady component P_s to the oscillatory pressure drop per unit length may be seen by comparing Figs. 7(a) and (b). Fig. 7(a) is the same as Fig. 5(c) and shows oscillatory flow and the experimental data of Thurston [38] (his Fig.5). In Fig. 7(b) P_s is chosen for each value of the rms oscillatory flow rate amplitude U to give $U_s = 1.95 \times 10^{-4}\text{cm}^3\text{s}^{-1}$. By adding this steady pressure drop it may be seen that the magnitude of P'' is quite dramatically reduced for the smallest values of U. This is because the imposition of an additional shear rate across the tube breaks up the aggregates and results in a less elastic fluid. The reader is referred to the paper of Vlastos et al. [39] (and to Figs. 1 and 2 of that paper, in particular), for further discussion of the effect on η'' of superimposing a steady shear rate on small amplitude oscillatory flow.

In Fig. 8 (a)-(f) we plot snapshots of the average aggregate size n, the polymeric viscosity $N_0 k_B T \mu$ and the axial velocity v_z as functions of the tube radius at four equally spaced points in time during a complete oscillatory cycle. For all plots $U_s = 1.95 \times 10^{-4}\text{cm}^3\text{s}^{-1}$. The figures in the left hand column correspond to a superimposed rms volume flow rate amplitude of $U = 1.2772 \times 10^{-5}\text{cm}^3\text{s}^{-1}$ and those on the right to a superimposed rms volume flow rate amplitude of $U = 9.63 \times 10^{-3}\text{cm}^3\text{s}^{-1}$. The general trend with U is the same as in Fig. 6 except that the non-zero volume flow rate over one cycle contributes to a slight further decrease in n and the polymeric viscosity compared to the purely oscillatory ($U_s = 0$) case.

Interestingly, Thurston [38] reported that there was no pronounced difference in the steady pressure due to increase in the amplitude of the oscillatory flow. In Fig.9 we show, in contrast, the value of P_s in the experiment of Fig. 7(b) required to maintain a volume flow rate of $U_s = 1.95 \times 10^{-4}\text{cm}^3\text{s}^{-1}$ over one cycle (that is, a time interval of length $2\pi/\omega$) for increasing values of the oscillatory amplitude U. Although the oscillatory part $\widetilde{U}$ of the volume flow rate contributes no net flow over one cycle its effect is to break up aggregates and reduce the local viscosity, leading to a smaller pressure drop being required to maintain the flow at the same volume rate. In other words, maintaining the same steady pressure drop per unit length P_s as U is increased will result in a progressive increase in the volume flow rate U_s. This so-called *flow enhancement* is well known in shear-thinning polymeric fluids and has been the subject of many earlier studies: see, for example, [2, 3, 13, 22, 23].

5. Conclusions

Tube flow of human blood has been shown to give rise to some complex non-Newtonian flow phenomena, the macroscopic manifestations of which (if not the phenomena themselves) may be observed in the laboratory: particle migration, reversible cell aggregation, shear-rate dependent viscoelasticity etc. The advantage of using the proposed mathematical model has been that explanations at the microstructural level are possible for what may be measured experimentally. Although simple, the model yields results that are in good agreement with the

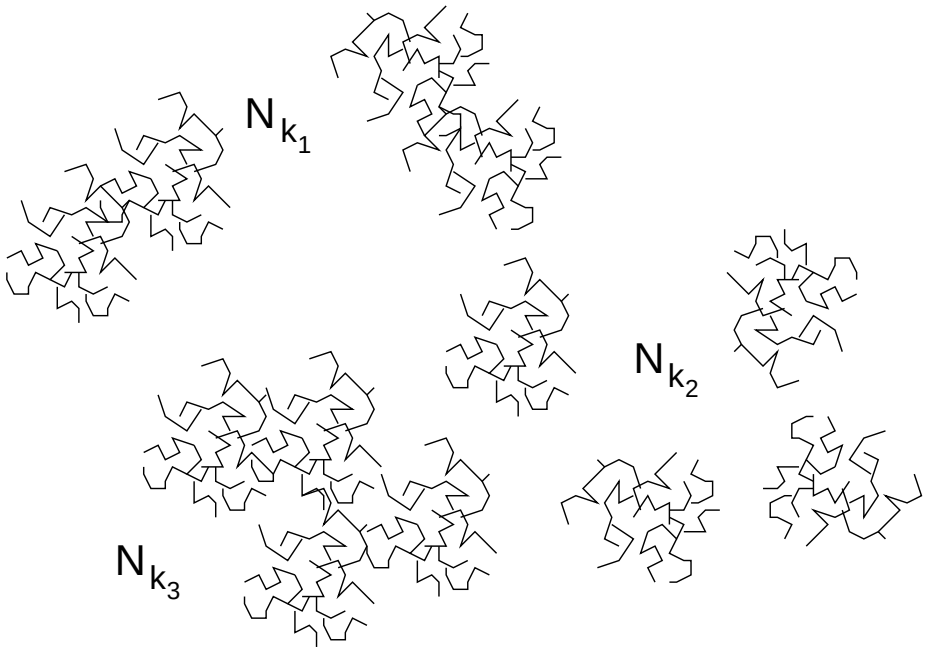

Figure 1: Diagrammatic representation of aggregates of sizes k_1, k_2 and k_3. N_{k_i} denotes the number of aggregates of size k_i $(i = 1, 2, 3)$.

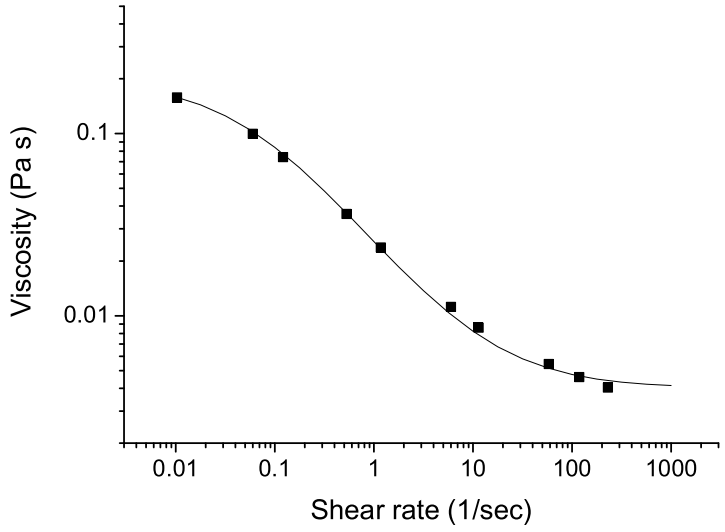

Figure 2: —— : steady state viscosity (47) and ■ : experimental data of Chien [10].

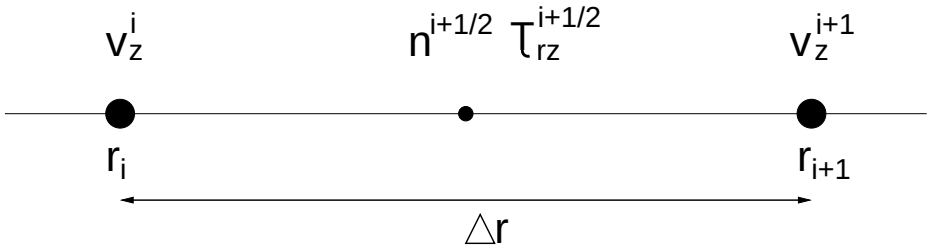

Figure 3: Staggered finite difference grid, showing arrangement of the dependent variables v_z^i, $n^{i+1/2}$, $\tau_{rz}^{i+1/2}$.

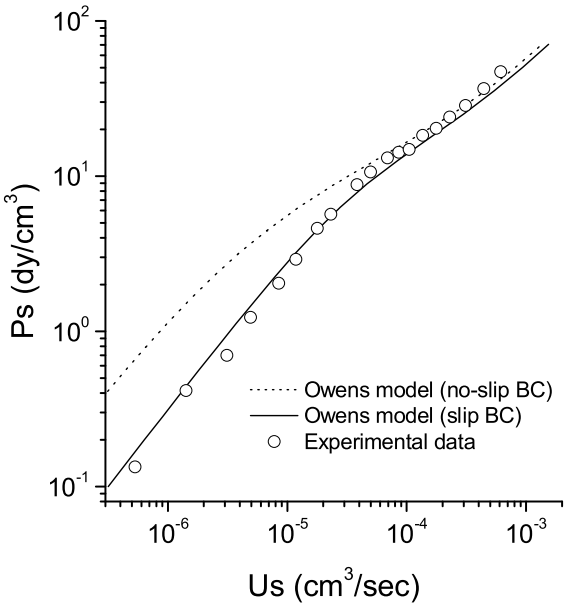

Figure 4: Steady flow. Pressure drop per unit length P_s against volume flow rate U_s with no-slip $\beta = 0$ and slip $\beta = 0.002$ velocity boundary conditions (41).

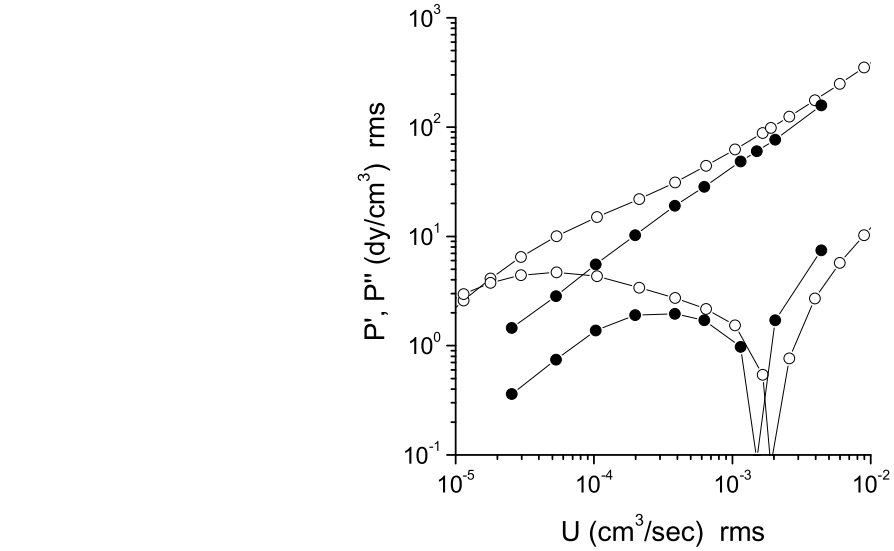

(a)

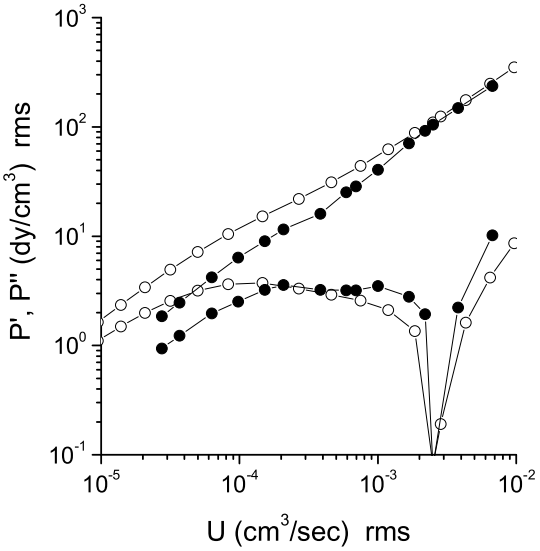

(b)

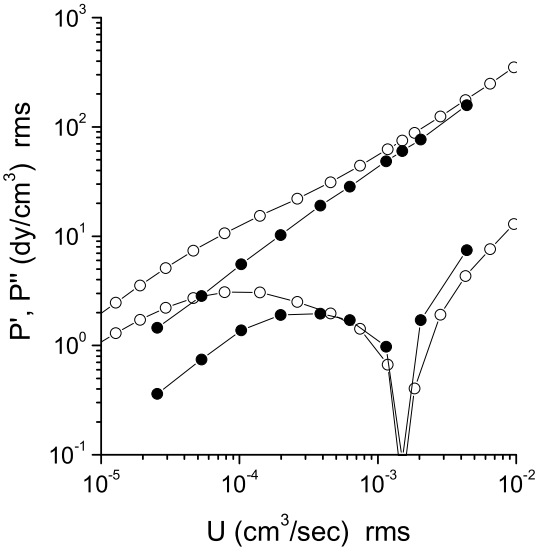

(c)

Figure 5: Oscillatory flow. rms pressure components in phase (P', upper curves) and in quadrature ($-P''$ and P'', lower curves) with $\widetilde{U}$ (see (34)). U is the rms amplitude of $\widetilde{U}$ (see (53)). (a) $\bullet$: experimental data from Thurston ([38], Fig. 5 "off") and $\circ$: computed results with no-slip boundary condition ($\beta = 0$ in (41)) (b) $\bullet$: experimental data from Thurston ([38], Fig. 3) and $\circ$: computed results with slip boundary condition ($\beta = 0.002$ in (41)) (c) $\bullet$: experimental data from Thurston ([38], Fig. 5 "off") and $\circ$: computed results with slip boundary condition ($\beta = 0.002$ in (41)).

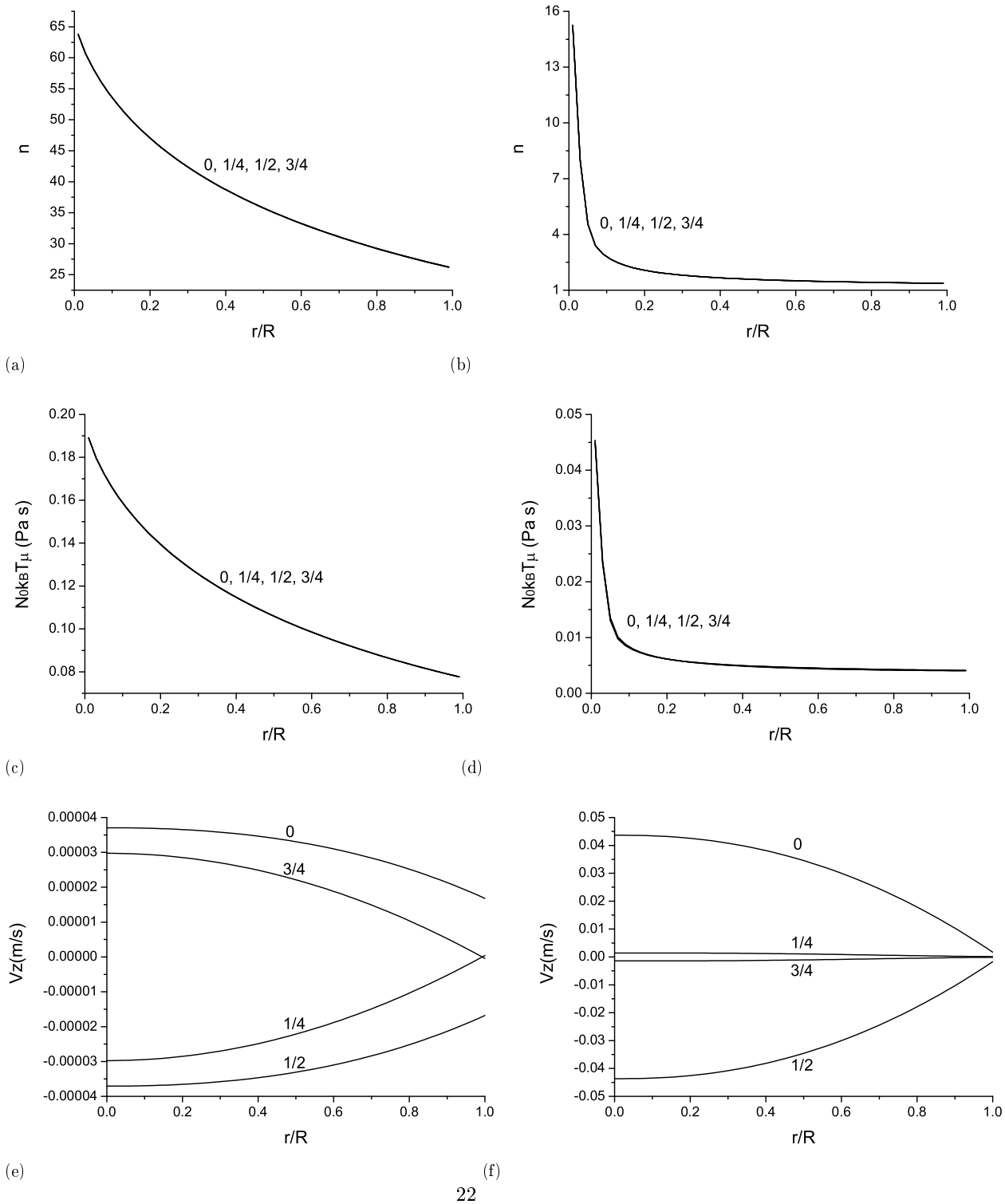

Figure 6: Oscillatory flow. $U = 1.2772 \times 10^{-5}\mathrm{cm}^3\mathrm{s}^{-1}$ (Figs. (a), (c), (e)) and $U = 9.63 \times 10^{-3}\mathrm{cm}^3\mathrm{s}^{-1}$ (Figs. (b), (d), (f)). (a) and (b): n, (c) and (d): polymeric viscosity $N_0 k_B T \mu$, (e) and (f): $v_z(r)$.

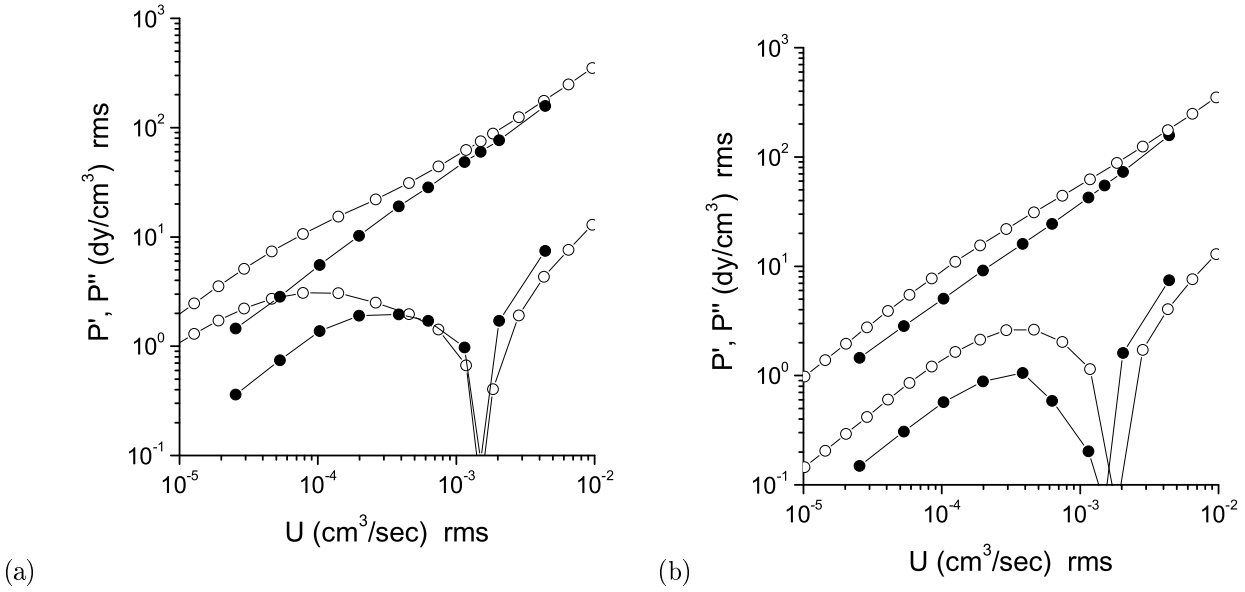

Figure 7: rms pressure components in phase (P', upper curves) and in quadrature ($-P''$ and P'', lower curves) with $\widetilde{U}$ (see (34)). U is the rms amplitude of $\widetilde{U}$ (see (53)). (a) Oscillatory flow. $\bullet$: experimental data from Thurston ([38], Fig. 5 "off") and $\circ$: computed results with slip boundary condition ($\beta = 0.002$ in (41)) (b) Pulsatile flow with $U_s = 1.95 \times 10^{-4}\mathrm{cm}^3\mathrm{s}^{-1}$. $\bullet$: experimental data from Thurston ([38], Fig. 5 "on") and $\circ$: computed results with slip boundary condition ($\beta = 0.002$ in (41)).

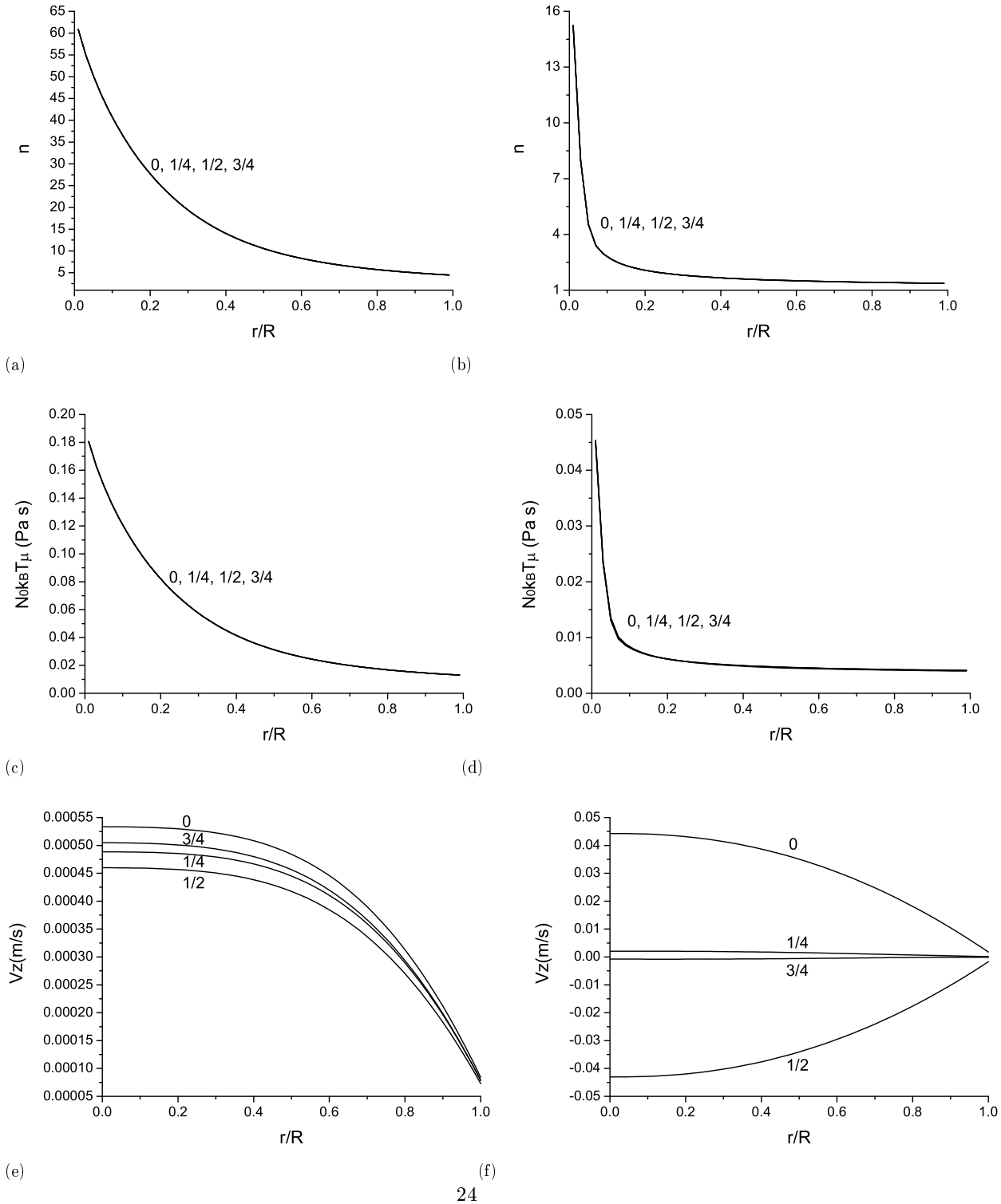

Figure 8: Pulsatile flow. $U_s = 1.95 \times 10^{-4}\mathrm{cm}^3\mathrm{s}^{-1}$. $U = 1.2772 \times 10^{-5}\mathrm{cm}^3\mathrm{s}^{-1}$ (Figs. (a), (c), (e)) and $U = 9.63 \times 10^{-3}\mathrm{cm}^3\mathrm{s}^{-1}$ (Figs. (b), (d), (f)). (a) and (b): n, (c) and (d): polymeric viscosity $N_0 k_B T \mu$, (e) and (f): $v_z(r)$

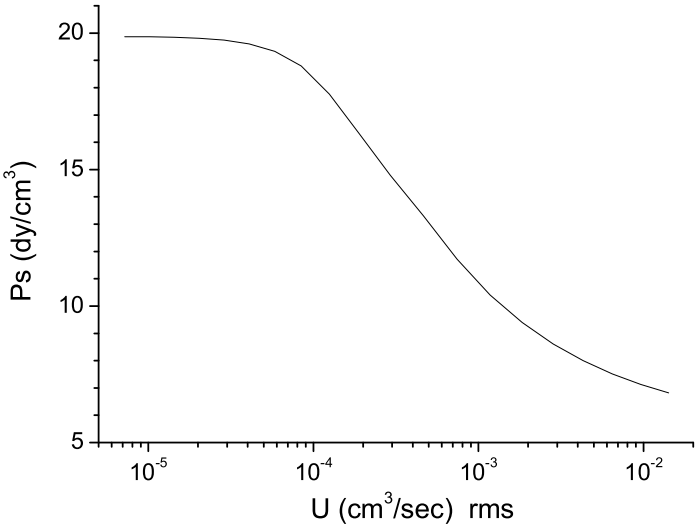

Figure 9: Flow enhancement in pulsatile flow. Pressure drop per unit length P_s required to maintain volume flow rate $U_s = 1.95 \times 10^{-4}\text{cm}^3\text{s}^{-1}$. U is the rms amplitude of $\widetilde{U}$ (see (53)).

available experimental data. The lubricating effect of the cell-depleted region near vessel walls has been accounted for with a Navier-type slip condition and the effect of this upon the bulk flow properties has been shown to be important. A weakness of the present implementation of the new constitutive model is that the red cell number density is a constant across the tube radius. Future work will allow red cell migration and therefore a non-uniform N_0. The polymer viscosity $N_0 k_B T \mu$ will then be allowed to vary in a natural way as a function of time, shear-rate and particle distribution.

A Parameter values

For nearly all computed results shown, the following parameter set was used:

$$\begin{aligned}
\text{fluid density, } \rho &= 1053.6\text{kg m}^{-3},\\
\text{plasma viscosity, } \eta_N &= 0.001\text{Pa s},\\
\text{zero shear-rate elastic viscosity, } \eta_0 &= 0.197\text{Pa s},\\
\text{high shear-rate elastic viscosity, } \eta_\infty &= 0.003\text{Pa s},\\
\text{Maxwell relaxation time, } \lambda_H &= 0.004\text{s},\\
a(\dot\gamma)N_0 \text{ model parameters (20), } c_1 &= 2.0\text{s}^{-1}, c_2 = 1.0, \dot\gamma_c = 5.78\text{s}^{-1},\\
\text{Slip coefficient (41), } \beta &= 0.002(\text{Pa s})^{-1}m,\\
\text{Cross model parameters (47), } m &= 0.75,\ \xi = 8.0\text{s}^m.
\end{aligned}$$

For the results of Fig. 5(b), $\lambda_H = 0.005$ s.

B Small amplitude oscillatory flow of a linear viscoelastic fluid

For small amplitude oscillatory flow we assume a linear viscoelastic model and write Eqn. (22) as

$$i\omega\rho v_z^* = \frac{\eta^*}{r}\frac{d}{dr}\left(r\frac{dv_z^*}{dr}\right) + P_M^* \exp(iA), \tag{60}$$

where, as explained in Section 4.2., η^* is a complex viscosity and the oscillatory negative pressure gradient is of the form (35). The solution to (60) satisfying the slip condition (see (41))

$$v_z^*(R) = -\beta\eta_e^*\frac{\partial v_z^*}{\partial r}(R), \tag{61}$$

is

$$v_z^*(r) = \frac{i}{\omega\rho}P_M^* \exp(iA)\left[\frac{J_0(Kr)}{J_0(KR) - K\beta\eta_e^* J_1(KR)} - 1\right], \tag{62}$$

where $\eta_e^* = \eta^* - \eta_N$, J_ν denotes the νth Bessel function of the first kind and

$$K^2 = -i\omega\rho/\eta^*. \tag{63}$$

The above developments generalize those of Womersley [42] in the case of a Newtonian fluid and Thurston [37] in the case of a linear viscoelastic fluid with a no-slip ($\beta = 0$) condition.

From (54) we see that

$$U^* = 2\pi\int_{r=0}^{R} v_z^*(r)\, r\, dr = -\frac{i\pi R^2 P_M^* \exp(iA)}{\rho\omega}\left[1 - \frac{2J_1(KR)}{KR(J_0(KR) - K\beta\eta_e^* J_1(KR))}\right], \tag{64}$$

and, noting that $\exp(iA) = U^*/U_M$ we then have

$$U_M = -\frac{i\pi R^2 P_M^*}{\rho\omega}\left[1 - \frac{2J_1(KR)}{KR(J_0(KR) - KR\delta J_1(KR))}\right], \tag{65}$$

where we have introduced a non-dimensionalized complex slip coefficient δ, defined by

$$\delta = \frac{\beta\eta_e^*}{R}.$$

Complicated as the relation (65) may at first sight appear, a significant simplification is possible on the assumption that δ and the Womersley number $\alpha = |K|R = R\sqrt{\rho\omega/|\eta^*|}$ are small. In this case, inverting the relationship and retaining the leading order terms, the expression for P_M^* is as follows:

$$P_M^* = \frac{8U_M}{\pi R^4}(1 - 4\delta)\eta^* + \frac{4i\rho\omega U_M}{3\pi R^2}(1 - 2\delta). \tag{66}$$

Finally, after a number of straightforward manipulations, the real and imaginary parts of (66) may be written down as

$$P'_M = \frac{8U_M}{\pi R^4}\left[\eta' - \frac{4\beta}{R}(\eta'^2 - \eta''^2 - \eta_N\eta') - \frac{\rho\omega\beta R}{3}\eta''\right],$$

and

$$P''_M = \frac{8U_M}{\pi R^4}\left[-\eta'' + \frac{\rho\omega R^2}{6} + \frac{4\beta}{R}(2\eta' - \eta_N)\eta'' - \frac{\rho\omega\beta R}{3}(\eta' - \eta_N)\right],$$

respectively.

References

[1] M. Anand and K. R. Rajagopal, A shear-thinning viscoelastic fluid model for describing the flow of blood, *Int. J. Cardiovascular Medicine and Science* **4** (2004), 59-68.

[2] H. A. Barnes, P. Townsend and K. Walters, Flow of non-Newtonian liquids under a varying pressure gradient, *Nature* **224** (1969), 585-587.

[3] H. A. Barnes, P. Townsend and K. Walters, Pulsatile flow of non-Newtonian liquids, *Rheol. Acta* **10** (1971), 517-527.

[4] R. B. Bird, C. F. Curtiss, R. C. Armstrong and O. Hassager, *Dynamics of Polymeric Liquids, Volume 2, Kinetic Theory,* John Wiley & Sons, New York, 1987.

[5] M. Bureau, J. C. Healy, D. Bourgoin and M. Joly, Rheological hysteresis of blood at low shear rate, *Biorheology* **17** (1980), 191-203.

[6] C. G. Caro, T. J. Pedley, R. C. Schroter and W. A. Seed, *The Mechanics of the Circulation,* Oxford University Press, Oxford, 1978.

[7] N. Casson, A flow equation for pigment-oil suspensions of printing ink type, in: *Rheology of Disperse Systems*, C. C. Mills, ed., Pergamon, 1959, pp.84-102.

[8] C. F. Chan Man Fong and D. De Kee, Generalized network type constitutive equations, *Physica A* **218** (1995), 56-68.

[9] J. Chen and Z. Huang, Analytical model for effects of shear rate on rouleau size and blood viscosity, *Biophysical Chemistry* **58** (1996), 273-279.

[10] S. Chien, Shear dependence of effective cell volume as determinant of blood viscosity, *Science* **168** (1970), 977-979.

[11] S. Chien, R. G. King, R. Skalak, S. Usami and A. L. Copley, Viscoelastic properties of human blood and red cell suspensions, *Biorheology* **12** (1975), 341-346.

[12] M. M. Cross, Rheology of non-Newtonian fluids: a new flow equation for pseudoplastic systems, *J. Colloid Sci.* **20** (1965), 417-437.

[13] J. M. Davies, S. Bhumiratana and R. B. Bird, Elastic and inertial effects in pulsatile flow of polymeric liquids in circular tubes, *J. Non-Newtonian Fluid Mech.* **3** (1978), 237-259.

[14] F. H. El-Khatib and E. R. Damiano, Linear and nonlinear analyses of pulsatile blood flow in a cylindrical tube, *Biorheology* **40** (2003), 503-522.

[15] J. C. Healy and M. Joly, Rheological behavior of blood in transient flow, Biorheology **12** (1975), 335-340.

[16] D. N. Ku, Blood flow in arteries, *Annu. Rev. Fluid Mech.* **29** (1997), 399-434.

[17] D. W. Liepsch, Flow in tubes and arteries - a comparison, *Biorheology* **23** (1986), 395-433.

[18] X. Y. Luo and Z. B. Kuang, A study on the constitutive equation of blood, *J. Biomechanics* **25** (1992), 929-934.

[19] T. Murata and T. W. Secomb, Effects of shear rate on rouleau formation in simple shear flow, *Biorheology* **25** (1988), 113-122.

[20] P. Neofytou, Comparison of blood rheological models for physiological flow simulation, *Biorheology* **41** (2004), 693-714.

[21] R. G. Owens, A new microstructure-based constitutive model for human blood, *J. Non-Newtonian Fluid Mech.* (2006), to appear.

[22] N. Phan-Thien, On pulsating flow of polymeric fluids, *J. Non-Newtonian Fluid Mech.* **4** (1978), 167-176.

[23] N. Phan-Thien and J. Dudek, Pulsating flow revisited, *J. Non-Newtonian Fluid Mech.* **11** (1982), 147-161.

[24] G. Pontrelli, Pulsatile blood flow in a pipe, *Computers and Fluids* **27** (1998), 367-380.

[25] D. Quemada, Rheology of concentrated disperse systems III. General features of the proposed non-Newtonian model. Comparison with experimental data, *Rheol. Acta* **17** (1978), 643-653.

[26] D. Quemada, A rheological model for studying the hematocrit dependence of red cell-red cell and cell-protein interaction in blood, *Biorheology* **18** (1981), 501-514.

[27] D. Quemada, A non-linear Maxwell model of biofluids: application to normal human blood, *Biorheology* **30** (1993), 253-265.

[28] D. Quemada, Rheological modelling of complex fluids. I. The concept of effective volume fraction revisited, *Eur. Phys. J. AP* **1** (1998), 119-127.

[29] D. Quemada, Rheological modelling of complex fluids. IV. Thixotropic and "thixoelastic" behaviour. Start-up and stress relaxation, creep tests and hysteresis cycles, *Eur. Phys. J. AP* **5** (1999), 191-207.

[30] K. R. Rajagopal and A. R. Srinivasa, A thermodynamic framework for rate-type fluid models, *J. Non-Newtonian Fluid Mech.* **88** (2000), 207-227.

[31] C. M. Rodkiewicz, P. Sinha and J. S. Kennedy, On the application of a constitutive equation for whole human blood, *Trans ASME* **112** (1990), 198-206.

[32] J. S. Rosenblatt, *The Rheology of Human Blood: A Structured Fluid Approach Based on Rouleau Behavior*, PhD thesis, Department of Chemical Engineering, University of California, Berkeley, 1988.

[33] T. Shiga, K. Imaizumi, N. Harada and M. Sekiya, Kinetics of rouleaux formation using TV image analyzer. I. Human erythrocytes, *Am. J. Physiol.* **245** (1983), H252-H258.

[34] D. A. Steinman and C. A. Taylor, Flow imaging and computing: large artery hemodynamics, *Ann. Biomed. Eng.* **33** (2005), 1704-1709.

[35] N. Sun and D. De Kee, Simple shear, hysteresis and yield stress in biofluids, *Can. J. Chem. Eng.* **79** (2001), 36-41.

[36] C. A. Taylor and M. T. Draney, Experimental and computational methods in cardiovascular fluid mechanics, *Annu. Rev. Fluid Mech.* **36** (2004), 197-231.

[37] G. B. Thurston, Theory of oscillation of a viscoelastic fluid in a circular tube, *J. Acoust. Soc. Am.* **24** (1960), 210-213.

[38] G. B. Thurston, Elastic effects in pulsatile blood flow, *Microvasc. Res.* **9** (1975), 145-157.

[39] G. Vlastos, D. Lerche and B. Koch, The superposition of steady on oscillatory shear and its effect on the viscoelasticity of human blood and a blood-like model fluid, *Biorheology* **34** (1997), 19-36.

[40] F. J. Walburn and D. J. Schneck, A constitutive equation for whole human blood, *Biorheology* **13** (1976), 201-218.

[41] M. C. Williams, J. S. Rosenblatt and D. S. Soane, Theory of blood rheology based on a statistical mechanics treatment of rouleaux, and comparisons with data, *Intern. J. Polymeric Mater.* **21** (1993), 57-63.

[42] J. R. Womersley, Method for the calculation of velocity, rate of flow and viscous drag in arteries when the pressure gradient is known, *J. Physiol.* **127** (1955), 553-563.

[43] K. K. Yeleswarapu, *Evaluation of Continuum Models for Characterizing the Constitutive Behavior of Blood*, PhD thesis, University of Pittsburgh, Pittsburgh, PA 1996.

[44] K. K. Yeleswarapu, M. V. Kameneva, K. R. Rajagopal and J. F. Antaki, The flow of blood in tubes: theory and experiment, *Mech. Res. Comm.* **25** (1998), 257-262.

[45] J.-B. Zhang and Z.-B. Kuang, Study on blood constitutive parameters in different blood constitutive equations, *J. Biomechanics* **33** (2000), 355-360.